Inorganic Chemistry

Article

pubs.acs.org/IC

Ligand Effects on the Oxidative Addition of Halogens to (dpp-nacnac^{R})Rh(phdi)

David W. Shaffer, Scott A. Ryken, Ryan A. Zarkesh, and Alan F. Heyduk*

Department of Chemistry, University of California, Irvine, California 92697-2025, United States

Supporting Information

ABSTRACT: The treatment of (dpp-nacnac^{R})Rh(phdi) {(dpp-nacnac^{R})$^{-}$ = CH[C(R)(N-^{i}Pr$_2$C$_6$H$_3$)]$_2^{-}$; R = CH_3, CF_3; phdi = 9,10-phenanthrenediimine} with X_2 oxidants afforded octahedral rhodium(III) products in the case of X = Cl and Br. The octahedral complexes exhibit well-behaved cyclic voltammograms in which a two-electron reduction is observed to regenerate the initial rhodium(I) complex. When treated with I_2, (dpp-nacnac^{CH3})Rh(phdi) produced a square pyramidal η^1-I_2 complex, which was characterized by NMR and UV−vis spectroscopies, mass spectrometry, and X-ray crystallography. The more electron poor complex (dpp-nacnac^{CF3})Rh(phdi) reacted with I_2 to give a mixture of two products that were identified by ^{1}H NMR spectroscopy as a square pyramidal η^1-I_2 complex and an octahedral diiodide complex. Reaction of the square pyramidal (dpp-nacnac^{CH3})Rh(I_2)(phdi) with HBF_4 resulted in protonation of the (dpp-nacnac^{CH3})$^{-}$ backbone to provide an octahedral rhodium(III) diiodide species. These reactions highlight the impact that changes in the electron-withdrawing nature of the supporting ligands can have on the reactivity at the metal center.

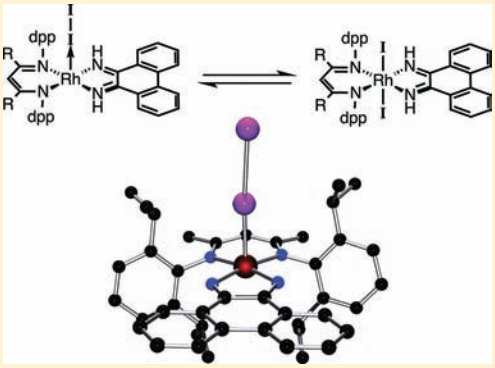

INTRODUCTION

Oxidative addition is a fundamental reaction of coordination complexes and is a key step in many catalytic reactions. Despite its importance, the exact mechanism of an oxidative addition reaction is often uncertain, and depends on the metal center, supporting ligands, substrate, and the relative concentrations of these species in solution.[1,2] The importance of oxidative addition in catalysis has prompted many studies to elucidate the electronic and steric factors that govern this reaction,[3,4] and a key aspect of these studies is the characterization of potential intermediates or transition states along the oxidative addition pathway.

The most common coordination platform for oxidative addition studies is the square-planar, 16-electron, d^8 metal complex.[1,5] The addition of halogen substrates to these complexes is generally thought to proceed through the formation of an η^1-X_2 adduct formed by donation of an electron pair from the metal into the σ^* orbital of X_2, leading to heterolytic cleavage of the X−X bond, as shown in Scheme 1.[6−10] A few complexes of platinum have been characterized that serve as models for the putative five-coordinate, η^1-adduct intermediate. A series of platinum(II) complexes of the 2,6-bis[(dimethylamino)methyl]phenyl ligand have been synthesized with an η^1-I_2 ligand,[11−15] as well as [Pt(dmpe)$_2$I(I_2)]I_3 (dmpe = 1,2-bis(dimethylphosphino)ethane).[16] Heterolytic cleavage of the X−X bond in one of these "intermediates" would generate a charge-separated complex,[10,17] which generally leads to the trans addition product,[9,10,18,19] though cis products have also been observed.[20] Isomerization often complicates mechanistic understanding in these reactions,[21] with mechanisms proposed in which the cis isomer forms first, followed by isomerization to the trans isomer,[9] and vice versa.[22,23] No models for analogous η^1-adducts exist for other catalytically significant metals such as rhodium, though I_2 has been shown to form a bridge between bimetallic rhodium(II) complexes.[24] The mechanism of X_2 addition to square planar Rh(I) complexes has also been shown to depend on the relative concentrations of the reactants.[25]

Scheme 1

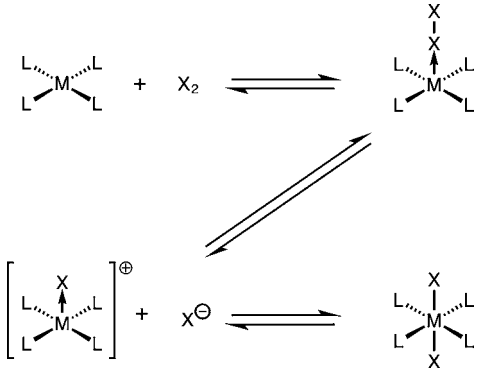

Previously, we reported the synthesis and redox properties of (dpp-nacnac^{R})Rh(phdi) {(dpp-nacnac^{R})$^{-}$ = CH[C(R)-

Received: April 9, 2012
Published: May 23, 2012

(N-^{i}Pr$_2$C$_6$H$_3$)]$_2^-$, phdi =9,10-phenanthrenediimine} complexes.[26] These complexes showed noninnocent electronic behavior owing to the juxtaposition of a low-valent rhodium(I) center and a reducible, redox-active, α-diimine ligand. Herein we report the reactivity of this rhodium platform with halogen oxidants. Chlorine and bromine react to give the expected rhodium(III) trans oxidative addition products, but iodine addition leads to an isolable η^1-adduct, (dpp-nacnac^R)Rh(I$_2$)-(phdi). It is shown that electronic substituents on the (dpp-nacnac^R)$^-$ ligand have a dramatic effect on the position of the equilibrium for the oxidative addition of I$_2$ to the rhodium center.

EXPERIMENTAL SECTION

General Considerations. Some of the complexes described below are air and moisture sensitive, necessitating that manipulations be carried out under an inert atmosphere of argon or nitrogen gas using standard Schlenk, vacuum-line, and glovebox techniques unless otherwise noted. Hydrocarbon solvents were sparged with nitrogen and then deoxygenated and dried by passage through Q5 and activated alumina columns, respectively. Ethereal and halogenated solvents were sparged with nitrogen and then dried by passage through two activated alumina columns. To test for effective oxygen and water removal, nonchlorinated solvents were treated with a few drops of a purple solution of sodium benzophenone ketyl in tetrahydrofuran (THF). (dpp-nacnac^R)Rh(phdi) (R = CH$_3$, **1a**; R = CF$_3$, **1b**) was prepared according to previously published procedures.[26] PhICl$_2$ was prepared according to literature procedures and used as a solid.[27] Bromine (Acros) was purified by distillation from P$_2$O$_5$, and iodine (EM Science) was purified by sublimation. Hydrochloric acid (EMD) and tetrafluoroboric acid (Alfa-Aesar) were used without further purification.

Electrochemical Methods. Electrochemical experiments were performed on a Gamry Series G 300 Potentiostat/Galvanostat/ZRA (Gamry Instruments, Warminster, PA, U.S.A.) using a 3.0 mm glassy carbon working electrode, a platinum wire auxiliary electrode, and a silver wire reference electrode. Electrochemical experiments were performed at room temperature, either in a glovebox or under an atmosphere of argon or nitrogen in a 1.0 mM analyte solution in THF with 0.10 M (n-Bu$_4$N)PF$_6$ as supporting electrolyte. All potentials are referenced to the Fc$^+$/Fc couple using decamethylferrocene as an internal standard at −0.49 V.[28] The typical solvent system window with our configuration was 1.5 V for the oxidation limit and −2.7 V for the reduction limit (vs the Fc$^+$/Fc couple). Decamethylferrocene (Acros) was purified by sublimation under reduced pressure and tetra-n-butylammonium hexafluorophosphate (Acros) was recrystallized from ethanol three times and dried under vacuum. To verify that electrode processes were diffusion-controlled, forward peak currents were plotted with respect to the square root of scan rates in the range of 50 to 1600 mV/s and found to be linear.

Physical Methods. NMR spectra were collected on Bruker Avance 400, 500, and 600 MHz spectrometers in dry, degassed CDCl$_3$. ^{1}H NMR spectra were referenced to TMS using the residual proteo impurities of the solvent; ^{13}C NMR spectra were referenced to TMS using the natural abundance ^{13}C impurities of the solvent. ^{19}F spectra were referenced to CFCl$_3$ using C$_6$F$_6$ as an internal standard at −164.9 ppm. All chemical shifts are reported using the standard notation in parts per million; positive chemical shifts are to a higher frequency from the given reference. Infrared spectra were recorded as KBr pellets with a Perkin-Elmer Spectrum One FTIR spectrophotometer. Electronic absorption spectra were recorded with Perkin-Elmer Lambda 800 and 900 UV−vis spectrophotometers. APCI-MS data was collected on a Waters LCT Premier mass spectrometer.

Synthesis of (dpp-nacnac^{CH3})RhCl$_2$(phdi) (2a). A solution of PhICl$_2$ (40.2 mg, 136 μmol, 1.0 equiv.) in 5 mL of CH$_2$Cl$_2$ was slowly added to a stirred dark blue solution of (dpp-nacnac^{CH3})Rh(phdi) (**1a**) (99.0 mg, 136 μmol, 1.0 equiv.) in 8 mL of CH$_2$Cl$_2$. The solution soon turned dark green and subsequently dark yellow-brown after stirring for 4 h at 25 °C. The volume was then reduced to 3 mL under reduced pressure and gently warmed to redissolve the solid. The solution was then layered with 7 mL of pentane. Dark brown crystals were isolated from the mother liquor, washed with pentane, and dried under vacuum providing **2a** in 85% yield (92 mg). Anal. Calcd. (Found) for C$_{43}$H$_{51}$N$_4$Cl$_2$Rh: C, 64.74 (64.73); H, 6.44 (6.62); N, 7.02 (6.97). ^{1}H NMR (600 MHz) δ/ppm: 10.02 (*s*, 2H, N−H), 8.00 (*d*, $^3J_{HH}$ = 8.1 Hz, 2H, aryl−H), 7.56 (*t*, $^3J_{HH}$ = 7.7 Hz, 2H, aryl−H), 7.44 (*t*, $^3J_{HH}$ = 7.6, 2H, aryl−H), 7.40−7.38 (*m*, 6H, aryl−H), 7.35 (*d*, $^3J_{HH}$ = 7.9 Hz, 2H, aryl−H), 5.06 (*s*, 1H, −CH−), 3.90 [*sept*, $^3J_{HH}$ = 6.7 Hz, 4H, −C*H*(CH$_3$)(CH$_3$)′], 2.17 (*s*, 6H, −CH$_3$), 1.32 [*d*, $^3J_{HH}$ = 6.5 Hz, 12H, −CH(C*H*$_3$)(CH$_3$)′], 1.15 [*d*, $^3J_{HH}$ = 6.8 Hz, 12H, −CH(CH$_3$)(C*H*$_3$)′]. ^{13}C{^{1}H} NMR (125.8 MHz) δ/ppm: 167.9 (CN), 161.5 (CN), 146.8 (aryl−C), 146.6 (aryl−C), 133.8 (aryl−C), 132.1 (aryl−C), 129.2 (aryl−C), 126.6 (aryl−C), 124.9, (aryl−C), 124.9 (aryl−C), 124.1 (aryl−C), 124.1 (aryl−C), 95.0 (−CH−), 28.6 [−CH(CH$_3$)(CH$_3$)′], 26.1 (−CH$_3$), 25.1 (−CH$_3$), 24.8 (−CH$_3$). IR (KBr) ν/cm^{-1}: 3285 (N−H), 1602 (C═N). UV−vis (CH$_2$Cl$_2$) λ_{max}/nm (ε/M^{-1} cm^{-1}): 282 (25,800), 296 (28,500), 350 (16,600), 941 (3,080). APCI-MS (toluene) m/z: 796.0 ([M]$^+$), 760.3 ([M − HCl]$^+$), 726.1 ([M − 2Cl]$^+$).

Synthesis of (dpp-nacnac^{CF3})RhCl$_2$(phdi) (2b). A 2 mL solution of PhICl$_2$ (24.7 mg, 89.8 μmol, 1.05 equiv.) in CH$_2$Cl$_2$ was added dropwise to a stirred 5 mL solution of (dpp-nacnac^{CF3})Rh(phdi) (**1b**) (71.5 mg, 85.7 μmol, 1 equiv.) in CH$_2$Cl$_2$ in air. The dark blue solution changed to dark green as it was stirred for 8 h. The solvent was removed, and the solid was washed with 2 × 10 mL of pentane, filtered, and dried, providing **2b** in 87% yield (67.4 mg). Anal. Calcd. (Found) for C$_{43}$H$_{45}$N$_4$F$_6$Cl$_2$Rh (%): C, 57.03 (56.70); H, 5.01 (4.77); N, 6.19 (5.97). ^{1}H NMR (400 MHz) δ/ppm: 9.81 (*s*, 2H, N−H), 8.01 (*d*, $^3J_{HH}$ = 7.8 Hz, 2H, aryl−H), 7.62 (*t*, $^3J_{HH}$ = 7.7 Hz, 2H, aryl−H), 7.47 (*t*, $^3J_{HH}$ = 7.6 Hz, 2H, aryl−H), 7.39 (*br*, 6H, aryl−H), 7.29 (*dd*, $^3J_{HH}$ = 7.9 Hz, $^4J_{HH}$ = 1.1 Hz, 2H, aryl−H), 5.53 (*s*, 1H, −CH−), 3.75 [*sept*, $^3J_{HH}$ = 6.7 Hz, 4H, −C*H*(CH$_3$)(CH$_3$)′], 1.35 [*d*, $^3J_{HH}$ = 6.5 Hz, 12H, −CH(C*H*$_3$)(CH$_3$)′], 1.15 [*d*, $^3J_{HH}$ = 6.9 Hz, 12H, −CH(CH$_3$)-(C*H*$_3$)′]. ^{13}C{^{1}H} NMR (125.8 MHz) δ/ppm: 168.7 (CN), 151.5 (q, $^2J_{CF}$ = 28.7 Hz, NC−CF$_3$), 145.5 (aryl−C), 145.1 (aryl−C), 134.8 (aryl−C), 132.6 (aryl−C), 129.5 (aryl−C), 127.2, (aryl−C), 125.2 (aryl−C), 124.4 (aryl−C), 124.4 (aryl−C), 124.4 (aryl−C), 119.4 (q, $^1J_{CF}$ = 285.6 Hz, −CF$_3$), 90.4 (−CH−), 29.0 [−CH(CH$_3$)(CH$_3$)′], 26.0 [−CH(CH$_3$)(CH$_3$)′], 25.0 [CH(CH$_3$)(CH$_3$)′]. ^{19}F NMR (376.5 MHz) −62.3 (s, 6F, −CF$_3$). IR (KBr) ν/cm^{-1}: 3295 (N−H), 1602 (C═N). UV−vis (CH$_2$Cl$_2$) λ_{max}/nm (ε/M^{-1} cm^{-1}): 278 (25,900), 293 (23,200), 354 (12,400), 437 (7,950), 713 (2,530). APCI-MS (toluene) m/z: 904.1 ([M]$^+$), 869.1 ([M − Cl]$^+$), 834.2 ([M − 2Cl]$^+$).

Synthesis of (dpp-nacnac^{CH3})RhBr$_2$(phdi) (3a). A CH$_2$Cl$_2$ solution of Br$_2$ (378 μL, 0.488 M, 184 μmol, 1 equiv.) was added slowly to a dark blue solution of **1a** (134 mg, 184 μmol, 1 equiv.) in 12 mL of CH$_2$Cl$_2$. After stirring at room temperature for 4 h, the volume of the dark green-brown solution was reduced to 3 mL, warmed briefly to redissolve the solid, and layered with 7 mL of pentane. Dark orange crystals were isolated from the mother liquor, washed with pentane, and dried under vacuum providing **3a** in 81% yield (132 mg). Anal. Calcd. (Found) for C$_{43}$H$_{51}$N$_4$Br$_2$Rh (%): C, 58.25 (58.53); H, 5.80 (5.95); N, 6.32 (6.29). ^{1}H NMR (600 MHz) δ/ppm: 10.18 (*s*, 2H, N−H), 7.98 (*d*, $^3J_{HH}$ = 8.0 Hz, 2H, aryl−H), 7.52 (*m*, 2H, aryl−H), 7.42−7.35 (*m*, 10H, aryl−H), 5.10 (*s*, 1H, −CH−), 4.00 [*sept*, $^3J_{HH}$ = 6.6 Hz, 4H, −C*H*(CH$_3$)(CH$_3$)′], 2.15 (*s*, 6H, CH$_3$), 1.39 [*d*, $^3J_{HH}$ = 6.5 Hz, 12H, −CH(C*H*$_3$)(CH$_3$)′], 1.16 [*d*, $^3J_{HH}$ = 6.7 Hz, 12H, −CH(CH$_3$)(C*H*$_3$)′]. ^{13}C{^{1}H} NMR (125.8 MHz) δ/ppm: 168.2 (CN), 162.6 (CN), 146.8 (aryl−C), 146.5 (aryl−C), 133.8 (aryl−C), 132.0 (aryl−C), 129.1 (aryl−C), 126.8 (aryl−C), 125.1, (aryl−C), 124.8 (aryl−C), 124.2 (aryl−C), 124.1 (aryl−C), 97.0 (−CH−), 28.8 [−CH(CH$_3$)(CH$_3$)′], 26.0 (−CH$_3$), 25.6 (−CH$_3$), 25.0 (−CH$_3$). IR (KBr) ν/cm^{-1}: 3284 (N−H), 1603 (C═N). UV−vis (CH$_2$Cl$_2$) λ_{max}/nm (ε/M^{-1} cm^{-1}): 300 (20,800), 359 (18,600), 599 (975), 961 (1,220). APCI-MS (toluene) m/z: 883.9 ([M]$^+$), 803.9 ([M − HBr]$^+$), 726.0 ([M − 2Br]$^+$).

dx.doi.org/10.1021/ic300733j | Inorg. Chem. 2012, 51, 12122−12131

Table 1. X-ray Diffraction Data-Collection and Refinement Parameters for (dpp-nacnac^{CH3})Rh(phdi) (1a), (dpp-nacnac^{CH3})RhCl$_2$(phdi) (2a), (dpp-nacnac^{CF3})RhCl$_2$(phdi) (2b), (dpp-nacnac^{CF3})RhBr$_2$(phdi) (3b), and (dpp-nacnac^{CH3})Rh(I$_2$)(phdi) (4a)

	(1a)	(2a)	(2b)	(3b)	(4a)
empirical formula	$C_{43}H_{51}N_4Rh\cdot C_3H_7NO$	$C_{43}H_{51}Cl_2N_4Rh$	$C_{43}H_{45}N_4Cl_2F_6Rh$	$C_{43}H_{49}N_4Br_2F_6Rh\cdot(CH_2Cl_2)_2$	$C_{43}H_{51}N_4I_2Rh\cdot(CH_2Cl_2)_2$
formula weight	799.88	797.69	905.64	1164.41	1150.44
crystal system	monoclinic	orthorhombic	orthorhombic	monoclinic	monoclinic
space group	*C*2/*c*	*Pbca*	*Pbca*	*P*2$_1$/*n*	*P*2$_1$/*n*
a/Å	45.474(2)	19.0502(10)	16.7113(16)	16.4697(5)	11.7200(14)
b/Å	8.9507(5)	19.3893(10)	17.8371(17)	13.4993(4)	20.000(2)
c/Å	23.6102(12)	21.0914(11)	26.507(3)	22.0254(7)	20.356(2)
α/deg	90	90	90	90	90
β/deg	120.7445(5)	90	90	107.6889(4)	100.673(2)
γ/deg	90	90	90	90	90
V/Å^3	8259.3(8)	7790.5(7)	7901.2(13)	4665.4(2)	4688.9(10)
Z	8	8	8	4	4
refl. collected	46503	85544	91644	54908	53029
indep. refl.	9798	9417	10105	11401	11275
*R*1 ($I > 2\sigma$)[a]	0.0297	0.0224	0.0365	0.0223	0.0281
w*R*2 (all data)[a]	0.0709	0.0616	0.0835	0.0559	0.0685

[a] $R_1 = \sum||F_o| - |F_c||/\sum|F_o|$; $wR_2 = [\sum w(F_o^2 - F_c^2)^2/\sum w(F_o^2)^2]^{1/2}$; GOF = $[\sum w(|F_o| - |F_c|)^2/(n - m)]^{1/2}$.

Synthesis of (dpp-nacnac^{CF3})RhBr$_2$(phdi) (3b). In air, **1b** (96.4 mg, 115 μmol, 1 equiv.) was dissolved in 10 mL of CH_2Cl_2 and treated dropwise with a $CHCl_3$ solution of Br_2 (3.48 mL, 33.3 mM, 116 μmol, 1 equiv.). The resulting green-brown solution was stirred for 5 h after which the solvent was removed in vacuo. The green-brown solid was washed with 4 × 4 mL of pentane, filtered, and dried in vacuo affording **3b** in 92% yield (105.1 mg). Anal. Calcd. (Found) for $C_{43}H_{45}N_4F_6Br_2Rh$ (%): C, 51.93 (52.13); H, 4.56 (4.45); N, 5.63 (5.49). ^{1}H NMR (500 MHz) *δ*/ppm: 9.98 (*s*, 2H, N−H), 8.03 (*d*, $^3J_{HH}$ = 8.1 Hz, 2H, aryl−H), 7.61 (*t*, $^3J_{HH}$ = 7.7 Hz, 2H, aryl−H), 7.48 (*t*, $^3J_{HH}$ = 7.6 Hz, 2H, aryl−H), 7.40−7.38 (m, 8H, aryl−H), 5.56 (s, 1H, −CH−), 3.83 [sept, $^3J_{HH}$ = 6.5 Hz, 4H, −C*H*(CH$_3$)(CH$_3$)′], 1.42 [*d*, $^3J_{HH}$ = 6.5 Hz, 12H, −CH(C*H*$_3$)(CH$_3$)′], 1.16 [*d*, $^3J_{HH}$ = 6.8 Hz, 12H, −CH(CH$_3$)(C*H*$_3$)′]. ^{13}C{^{1}H} NMR (125.8 MHz) *δ*/ppm: 168.9 (CN), 152.5 (q, $^2J_{CF}$ = 28.1 Hz, NC−CF$_3$), 145.7 (aryl−C), 144.7 (aryl−C), 134.7 (aryl−C), 132.4 (aryl−C), 129.4 (aryl−C), 127.3, (aryl−C), 125.4 (aryl−C), 124.5 (aryl−C), 124.4 (aryl−C), 124.3 (aryl−C), 119.2 (q, $^1J_{CF}$ = 285.9 Hz, −CF$_3$), 92.6 (−CH−), 29.2 [−CH(CH$_3$)(CH$_3$)′], 26.0 [−CH(CH$_3$)(CH$_3$)′], 25.2 [−CH(CH$_3$)-(CH$_3$)′]. ^{19}F NMR (376.5 MHz) −62.5 (s, −CF$_3$). IR (KBr) *ν*/cm^{-1}: 3272 (N−H), 1602 (C═N). UV−vis (CH_2Cl_2) λ_{max}/nm (ε/M^{-1} cm^{-1}): 299 (17,100), 365 (14,500), 447 (6,840), 738 (2,520). APCI-MS (toluene/CH_2Cl_2) *m*/*z*: 992.1 ([M]$^+$), 913.1 ([M − Br]$^+$), 834.2 ([M − 2Br]$^+$), 833.2 ([M − Br$_2$H]$^+$)

Synthesis of (dpp-nacnac^{CH3})Rh(I$_2$)(phdi) (4a). A solution of I_2 (25.8 mg, 102 μmol, 1 equiv.) in 6 mL of CH_2Cl_2 was added dropwise to a stirred solution of **1a** (75.0 mg, 103 μmol, 1 equiv.) in 4 mL of CH_2Cl_2. The solution was stirred 1 day; then the solvent was reduced to approximately 1.5 mL. Pentane (10 mL) was added to precipitate the product which was filtered, washed with an additional 5 × 2 mL of pentane, and dried in vacuo to provide **4a** in 97% yield (97.6 mg). ^{1}H NMR (600 MHz, 223K) *δ*/ppm: 8.86 (s, 2H, N−H), 8.11 (*d*, $^3J_{HH}$ = 8.4 Hz, 2H, aryl−H), 7.63 (*t*, $^3J_{HH}$ = 7.6 Hz, 2H, aryl−H), 7.58−7.53 (*m*, 4H, aryl−H), 7.41 (*t*, $^3J_{HH}$ = 6.9 Hz, 2H, aryl−H), 7.23 (*d*, $^3J_{HH}$ = 6.6 Hz, 2H, aryl−H), 7.00 (*br*, 2H, aryl−H), 5.71 (*s*, 1H, −CH−), 3.93 [*br*, 2H, −C*H*(CH$_3$)(CH$_3$)′], 2.43 [*br*, 2H, −C*H*(CH$_3$)(CH$_3$)′], 2.22 (*s*, 6H, −CH$_3$), 1.48 (*d*, $^3J_{HH}$ = 5.4 Hz, 6H, −CH(C*H*$_3$)(CH$_3$)′), 1.38 [*d*, 6H, −CH(CH$_3$)(C*H*$_3$)′], 0.95 [*d*, 6H, −CH(C*H*$_3$)(CH$_3$)′], 0.74 [*d*, 6H, −CH(CH$_3$)(C*H*$_3$)′]. IR (KBr) *ν*/cm^{-1}: 3305 (N−H), 1601 (C═N). UV−vis (CH_2Cl_2) λ_{max}/nm (ε/M^{-1} cm^{-1}): 292 (22,400), 358 (27,700), 461 (11,900), 530 (8,300), 600 (7,090), 684 (7,830), 789 (9,920). APCI-MS (toluene) *m*/*z*: 853.2 ([M − HI]$^+$), 726.3 ([M − 2I]$^+$).

Reaction of (dpp-nacnac^{CF3})Rh(phdi) with I$_2$. A sample of **1b** (80.3 mg, 96.2 μmol, 1 equiv.) was dissolved in 10 mL of CH_2Cl_2. I_2 (24.3 mg, 95.7 μmol, 1 equiv.) was dissolved in dry 6 mL of CH_2Cl_2 and added dropwise to the stirred **1b** solution under a positive flow of nitrogen. The dark blue solution became brown, and the reaction mixture was stirred for 12 h after which the solvent was removed. The brown solid was washed with 5 × 2 mL of pentane, filtered in air, and dried, resulting in a mixture of η^1-I$_2$ and *trans*-I$_2$ isomers **4b** and **5b**, respectively, in 90% yield (93.3 mg). IR (KBr) *ν*/cm^{-1}: 3295 (N−H), 1602 (C═N).

Synthesis of [(dpp-nacnacH^{CH3})RhCl$_2$(phdi)][Cl] ([6a][Cl]). To a dark brown solution of **3a** (111 mg, 139 μmol) in CH_2Cl_2 (10 mL) in air was added 0.5 mL of 12.1 N HCl$_{(aq)}$, causing a color change to bright red-orange. Hexanes (30 mL) were added to precipitate the product as a bright orange solid, which was isolated by filtration, washed with water (5 mL) and hexanes (5 mL), and dried in vacuo to provide [**6a**][Cl] in 87% yield (101.6 mg). Anal. Calcd. (Found) for $C_{43}H_{52}N_4Cl_3Rh\cdot H_3OCl$: C, 58.12 (58.16); H, 6.24 (6.17); N, 6.30 (6.27). ^{1}H NMR (600 MHz) *δ*/ppm: 9.88 (*s*, 2H, N−H), 8.08 (*d*, $^3J_{HH}$ = 8.1 Hz, 2H, aryl−H), 7.72 (*t*, $^3J_{HH}$ = 7.7 Hz, 2H, aryl−H), 7.55−7.49 (*m*, 8H, aryl−H), 7.35 (*d*, $^3J_{HH}$ = 8.0 Hz, 2H, aryl−H), 5.72 (*s*, 2H, −CH$_2$−), 3.37 [*sept*, $^3J_{HH}$ = 6.6 Hz, 4H, −C*H*(CH$_3$)(CH$_3$)′], 2.87 (*s*, 6H, −CH$_3$), 1.36 [*d*, $^3J_{HH}$ = 6.5 Hz, 12H, −CH(C*H*$_3$)(CH$_3$)′], 1.18 [*d*, $^3J_{HH}$ = 6.7 Hz, 12H, −CH(CH$_3$)(C*H*$_3$)′]. ^{13}C{^{1}H} NMR (125.8 MHz) *δ*/ppm: 183.6 (C═N), 169.6 (C═N), 142.8 (aryl−C), 142.5 (aryl−C), 136.0 (aryl−C), 133.1 (aryl−C), 130.1 (aryl−C), 129.2 (aryl−C), 125.5, (aryl−C), 125.4 (aryl−C), 124.9 (aryl−C), 123.9 (aryl−C), 49.4 (−CH$_2$−), 29.1 (−CH$_3$), 29.1 [−CH(CH$_3$)(CH$_3$)′], 26.4 (−CH$_3$), 24.2 (−CH$_3$). IR (KBr) *ν*/cm^{-1}: 3285 (N−H), 1659 (C═N), 1601 (C═N). UV−vis (CH_2Cl_2) λ_{max}/nm (ε/M^{-1} cm^{-1}): 291 (17,200), 300 (19,200), 359 (11,000), 470 (4,100). APCI-MS (toluene/CH_2Cl_2) *m*/*z*: 797.1 ([M]$^+$), 796.1 ([M − H]$^+$), 726.1 ([M − 2HCl]$^+$).

Synthesis of [(dpp-nacnacH^{CH3})RhCl$_2$(phdi)][BF$_4$] ([6a][BF$_4$]). In air, a dark brown 4 mL solution of **2a** (22.2 mg, 27.8 μmol, 1 equiv.) in CH_2Cl_2 was treated with one drop of neat $HBF_4\cdot OEt_2$. The resulting light orange solution was stirred for 30 min after which 10 mL of pentane was added to effect precipitation of the bright orange product, which was filtered, washed with 3 × 2 mL of ether, and dried under vacuum affording [**6a**][BF$_4$] in 87% yield (21.5 mg). ^{1}H NMR (600 MHz) *δ*/ppm: 9.87 (*s*, 2H, N−H), 8.08 (*d*, $^3J_{HH}$ = 8.2 Hz, 2H, aryl−H), 7.72 (*t*, $^3J_{HH}$ = 7.7 Hz, 2H, aryl−H), 7.55−7.50 (*m*, 8H, aryl−H), 7.35 (*d*, $^3J_{HH}$ = 8.0 Hz, 2H, aryl−H), 5.10 (*s*, 2H, −CH$_2$−), 3.38 [*sept*, $^3J_{HH}$ = 6.6 Hz, 4H, −C*H*(CH$_3$)(CH$_3$)′], 2.70 (*s*, 6H,

dx.doi.org/10.1021/ic300733j | Inorg. Chem. 2012, 51, 12122−12131

$-CH_3$), 1.37 (*d*, $^3J_{HH}$ = 6.5 Hz, 12H, $-CH(CH_3)(CH_3)'$), 1.18 (*d*, $^3J_{HH}$ = 6.7 Hz, 12H, $-CH(CH_3)(CH_3)'$). $^{13}C\{^1H\}$ NMR (125.8 MHz) δ/ppm: 183.1 (C=N), 169.6 (C=N), 142.7 (aryl−C), 142.6 (aryl−C), 136.1 (aryl−C), 133.1 (aryl−C), 130.1 (aryl−C), 129.2 (aryl−C), 125.5 (aryl−C), 125.4 (aryl−C), 124.9 (aryl−C), 123.9 (aryl−C), 48.9 ($-CH_2-$), 29.0 [$-CH(CH_3)(CH_3)'$], 28.3 ($-CH_3$), 26.4 ($-CH_3$), 24.2 ($-CH_3$). IR (KBr) ν/cm^{-1}: 3287 (N−H), 1656 (C=N), 1600 (C=N). APCI-MS (toluene/CH_2Cl_2) *m*/*z*: 797.2 ($[M]^+$), 796.2 ($[M - H]^+$), 795.2 ($[M - 2H]^+$), 761.2 ($[M - HCl]^+$), 760.2 ($[M - HClH]^+$), 726.2 ($[M - HCl_2]^+$), 725.2 ($[M - 2(HCl)]^+$).

Synthesis of [(dpp-nacnacH^{CH3})RhI$_2$(phdi)]BF$_4$ ([7a][BF$_4$]). Degassed $HBF_4{\cdot}OEt_2$ (96 μL, 0.74 M in CH_2Cl_2, 1.2 equiv.) was added to a dark green solution of **3a** (58.0 mg, 59.1 μmol, 1 equiv.) in 8 mL of CH_2Cl_2 and stirred for 15 min to afford a dark red-orange solution. Degassed hexane (15 mL) was added to effect product precipitation. The resulting suspension was filtered and washed with 10 mL of diethyl ether. The dark orange product was washed through the frit with 8 mL of CH_2Cl_2 and then dried in vacuo to yield [**7a**][BF_4] in 77% yield (48.6 mg).^{1}H NMR (600 MHz) δ/ppm: 10.16 (*s*, 2H, N−H), 8.13 (*d*, $^3J_{HH}$ = 8.1 Hz, 2H, aryl−H), 7.69 (*t*, $^3J_{HH}$ = 7.7 Hz, 2H, aryl−H), 7.59 (*t*, $^3J_{HH}$ = 7.5 Hz, 2H, aryl−H), 7.54−7.50 (*m*, 8H, aryl−H), 5.28 (*s*, 2H, $-CH_2-$), 3.55 [*br.*, 4H, $-CH(CH_3)(CH_3)'$], 2.66 (*s*, 6H, $-CH_3$), 1.54 [*d*, $^3J_{HH}$ = 6.2 Hz, 12H, $-CH(CH_3)(CH_3)'$], 1.20 [*d*, $^3J_{HH}$ = 6.6 Hz, 12H, $-CH(CH_3)(CH_3)'$]. $^{13}C\{^1H\}$ NMR (125.8 MHz) δ/ppm: 184.5 (C=N), 170.4 (C=N), 143.9 (aryl−C), 135.7 (aryl−C), 132.7 (aryl−C), 129.8 (aryl−C), 129.5 (aryl−C), 125.7 (aryl−C), 125.6 (aryl−C), 124.7 (aryl−C), 123.6 (aryl−C), 123.6 (aryl−C), 54.9 ($-CH_2-$), 29.8 [$-CH(CH_3)(CH_3)'$], 29.3 ($-CH_3$), 26.3 ($-CH_3$), 25.1 ($-CH_3$). IR (KBr) ν/cm^{-1}: 3281 (N−H), 1648 (C=N), 1601 (C=N).

Crystallographic Methods. X-ray diffraction data were collected on crystals mounted on glass fibers using a Bruker CCD platform diffractometer equipped with a CCD detector. Measurements were carried out at 163 K using Mo Kα (λ = 0.71073 Å) radiation, which was wavelength selected with a single-crystal graphite monochromator. The SMART program package was used to determine unit-cell parameters and to collect data. The raw frame data were processed using SAINT and SADABS to yield the reflection data files. Subsequent calculations were carried out using the SHELXTL program suite. Structures were solved by direct methods and refined on F^2 by full-matrix least-squares techniques. Analytical scattering factors for neutral atoms were used throughout the analyses. Hydrogen atoms were included using a riding model. ORTEP diagrams were generated using ORTEP-3 for Windows.[29] Diffraction data are shown in Table 1.

RESULTS

Halogen Oxidative Addition to (dpp-nacnac^R)Rh(phdi). The rhodium complex (dpp-nacnac^{CH3})Rh(phdi) (**1a**) has been characterized by single-crystal X-ray diffraction studies. Previously, we reported the synthesis, electrochemistry, and spectroscopic characterization of both **1a** and the fluorinated nacnac derivative, (dpp-nacnac^{CF3})Rh(phdi) (**1b**).[26] These complexes were characterized as having both rhodium(I)-diimine and rhodium(II)-diiminosemiquinonate character; however, informative structural data were missing for both complexes. Recently, crystals of **1a**, suitable for analysis by single-crystal X-ray diffraction methods, were obtained by cooling a saturated dimethylformamide (DMF) solution of **1a**. An ORTEP diagram of the complex is shown in Figure 1, and selected metrical data for the structure are given in Table 2. The bond distances between the rhodium center and the nitrogen atoms of the (dpp-nacnac^{CH3})$^-$ ligand are 1.99 Å, shorter than those in (dpp-nacnac^{CH3})Rh(CO)$_2$[26] and in (dpp-nacnac^{CH3})Rh(N$_2$)(cyclooctene),[30] but longer than the Rh−N bonds in (dpp-nacnac^{CH3})Rh(cyclooctene).[31] Rh−N$_{phdi}$ bond lengths of 1.97 Å in **1a** are almost exactly the same as those in

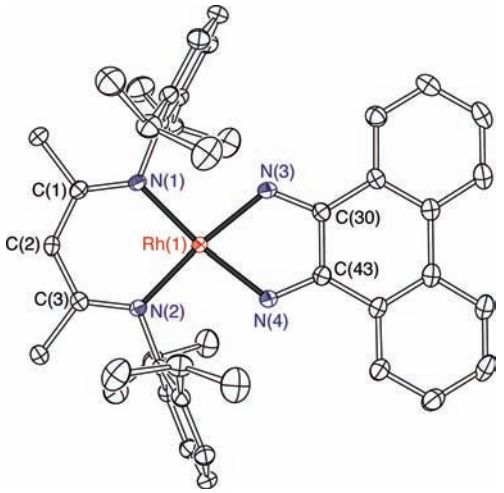

Figure 1. ORTEP diagram of (dpp-nacnac^{CH3})Rh(phdi) (**1a**). Thermal ellipsoids are shown at 50% probability. Hydrogen atoms and solvent molecules have been removed for clarity.

the isoelectronic complex (Cp*)Rh(HNC$_6$H$_4$NH).[32] The N−C distances within the phdi ligand of **1a** are significantly longer than the N−C distances within the phdi ligands in the rhodium(III) complexes **2a**, **2b**, and **3b**, described below. In the case of **1a**, the longer C−N bonds are consistent with a more electron-rich rhodium center, which results in significant donation of electron density from the rhodium center to the phdi ligand. In other words, Rh→phdi π backbonding is significant in **1a**, leading to partial reduction of the phdi ligand and partial oxidation of the rhodium center. The electronic structure of **1a** has been discussed in more detail previously.[26]

The formally rhodium(I) complexes **1a** and **1b** reacted with strong halogen oxidants to afford rhodium(III) oxidative addition products in high yields, as shown in Scheme 2. Addition of a CH_2Cl_2 solution of the chlorine delivery agent $PhICl_2$ to a dark blue solution of **1a** resulted in an initial color change to green and finally to yellow-brown. The product, (dpp-nacnac^{CH3})RhCl$_2$(phdi) (**2a**) was isolated by crystallization from a mixture of CH_2Cl_2 and pentane as brown crystals in 85% yield. An analogous reaction using Br_2 as the oxidant afforded the dibromide product, (dpp-nacnac^{CH3})RhBr$_2$(phdi) (**3a**), as a dark orange, crystalline solid in 81% yield. Similar reactivity was observed for the reactions of $PhICl_2$ and Br_2 with **1b**, which provided green (dpp-nacnac^{CF3})RhCl$_2$(phdi) (**2b**, 87% yield) and brown (dpp-nacnac^{CF3})RhBr$_2$(phdi) (**3b**, 92% yield), respectively.

Single-crystal X-ray diffraction studies on **2a** revealed an octahedral rhodium(III) complex generated by oxidative addition of chlorine to **1a**. Figure 2 shows the molecular structure of **2a**; Table 2 includes selected bond distances for the complex. The crystal structure of **2a** showed trans oxidative addition of chlorine to the rhodium center with the chloride ligands of the octahedron bound at typical Rh^{III}−Cl distances of 2.35 and 2.34 Å.[33−35] The dpp-nacnac^{CH3} and phdi ligands occupy the equatorial plane of the rhodium complex. The Rh−N distances to the (dpp-nacnac^{CH3})$^-$ and phdi ligands of 2.04 Å and 2.01 Å, respectively, are longer than those for square-planar **1a**, consistent with both increased steric crowding at the metal center and decreased π-backbonding from the rhodium center. Notably, the distances for the C=N (1.29 Å) and C−C (1.47 Å) bonds in the phdi ligand are consistent with the fully oxidized diimine form of the ligand.

dx.doi.org/10.1021/ic300733j | *Inorg. Chem.* 2012, 51, 12122−12131

Table 2. Selected bond distances (Å) and angles (deg) for (dpp-nacnac^{CH3})Rh(phdi) (1a), (dpp-nacnac^{CH3})RhCl$_2$(phdi) (2a), (dpp-nacnac^{CF3})RhCl$_2$(phdi) (2b), (dpp-nacnac^{CF3})RhBr$_2$(phdi) (3b), and (dpp-nacnac^{CH3})Rh(I$_2$)(phdi) (4a)

bond	(1a)	(2a)	(2b)	(3b)	(4a)
Rh–X(1)		2.3541(3)	2.3635(6)	2.5010(2)	2.6701(4)
Rh–X(2)		2.3395(3)	2.3108(6)	2.4721(2)	
X(1)–X(2)					3.0128(4)
Rh–N(1)	1.9920(14)	2.0455(11)	2.0762(18)	2.0720(14)	2.020(2)
Rh–N(2)	1.9894(14)	2.0449(12)	2.0684(17)	2.0795(14)	2.009(2)
Rh–N(3)	1.9689(15)	2.0149(12)	2.0161(18)	2.0086(14)	2.004(2)
Rh–N(4)	1.9773(15)	2.0082(12)	1.9901(18)	2.0051(14)	1.996(2)
N(1)–C(1)	1.337(2)	1.3242(17)	1.312(3)	1.319(2)	1.337(3)
N(2)–C(3)	1.334(2)	1.3218(18)	1.316(3)	1.313(2)	1.336(3)
C(1)–C(2)	1.398(2)	1.400(2)	1.402(3)	1.397(2)	1.399(4)
C(2)–C(3)	1.396(2)	1.400 (2)	1.391(3)	1.401(2)	1.395(4)
N(3)–C(30)	1.327(2)	1.2911(17)	1.289(3)	1.293(2)	1.309(3)
N(4)–C(43)	1.325(2)	1.2918(18)	1.293(3)	1.293(2)	1.311(3)
C(30)–C(43)	1.425(2)	1.4733(19)	1.477(3)	1.478(2)	1.457(3)
N(1)–Rh–N(2)	90.57(6)	90.12(4)	94.54(7)	92.07(5)	91.95(9)
N(3)–Rh–N(4)	76.77(6)	76.84(4)	77.10(7)	76.60(6)	76.69(9)
X(1)–Rh–X(2)		174.719(11)	177.67(2)	173.591(8)	
Rh–X(1)–X(2)					176.362(9)

Scheme 2

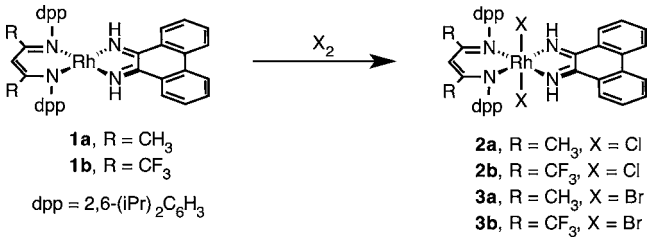

X-ray diffraction analysis of single crystals of **2b** and **3b** confirmed an octahedral geometry analogous to that of **2a**. Bond lengths for **2b** and **3b** are listed in Table 2. The Rh–N_{nacnac} bond distances in **2b** are approximately 0.02 Å longer than those in **2a**, and the C–N_{nacnac} distances are slightly shorter, consistent with the electron-withdrawing effect of the trifluoromethyl substituents. The Rh–N_{phdi} distances, as well as the bonds within the phdi ligand itself, are similar in **2a**, **2b**, and **3b**. The main difference between the structures of **2b** and **3b** is the slightly longer Rh–N_{nacnac} distances in **3b**, consistent with greater steric repulsion between the larger bromine atoms and the diisopropylphenyl groups. The Rh–Br bond distances in **3b** are typical for rhodium(III).[36,37]

Spectroscopic and mass spectrometric data for all derivatives of **2** and **3** indicate that the solid state structures observed for **2a**, **2b**, and **3b** are conserved in solution. Atmospheric-pressure chemical-ionization (APCI) mass spectrometry displayed an $[M]^+$ peak with the expected isotopic pattern for **2a** at 796.0 amu. Similarly, the APCI mass spectrum of **3a** showed the expected $[M]^+$ peak at 883.9 amu, and the spectra of **2b** and **3b** had consistent peaks at 904.1 and 992.1 amu, respectively. All four complexes showed fragmentation consistent with their molecular formulas. The ^{1}H NMR spectra of **2** and **3** suggest that the complexes have nominal C_{2v} symmetry in solution as indicated by a single sharp septet resonance for the methine proton of the isopropyl groups of the (dpp-nacnac^R)$^-$ ligands. The IR absorption spectra of all four compounds displayed a medium-intensity peak at 1602–1603 cm^{-1} which was not present in **1**, consistent with more double-bond character in the ligand C–N bonds from decreased Rh→phdi electron donation.

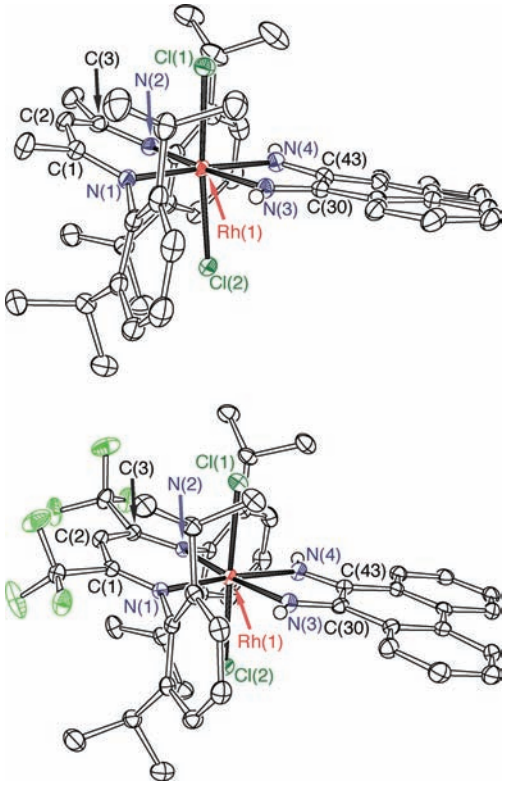

Figure 2. ORTEP diagrams of (dpp-nacnac^{CH3})RhCl$_2$(phdi) (**2a**) and (dpp-nacnac^{CF3})RhCl$_2$(phdi) (**2b**). Thermal ellipsoids are shown at 50% probability. Hydrogen atoms and solvent molecules have been removed for clarity.

The absorbance spectra of **2** and **3** are dominated by intense features in the near-UV and near-IR portions of the spectrum. Figure 3 shows the UV–vis–NIR spectra of **2** and **3** in CH_2Cl_2. Strong absorptions are observed for all four complexes in the near-UV region at 351 nm (**2a**), 359 nm (**2b**), 359 nm (**3a**), and 365 nm (**3b**). In both **2a** and **3a**, these transitions display

dx.doi.org/10.1021/ic300733j | Inorg. Chem. 2012, 51, 12122–12131

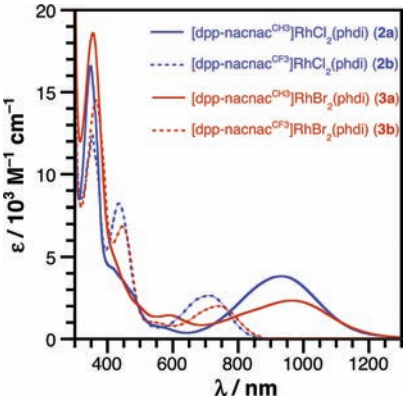

Figure 3. UV−vis absorption spectra of (dpp-nacnac^{CH3})RhCl$_2$(phdi) (**2a**), (dpp-nacnac^{CF3})RhCl$_2$(phdi) (**2b**), (dpp-nacnac^{CH3})-RhBr$_2$(phdi) (**3a**), and (dpp-nacnac^{CF3})RhBr$_2$(phdi) (**3b**) in CH_2Cl_2 at 25 °C.

shoulders in the 400 to 500 nm region, but in the fluorinated derivatives **2b** and **3b**, the shoulders are red-shifted to afford well-defined maxima at 437 and 447 nm, respectively. All four complexes also show relatively strong (ε = 2000−4000 M^{-1} cm^{-1}), broad absorptions in the near-IR portion of the spectrum (600−1200 nm). The lowest energy absorption for **2a** appears at 941 nm and substitution of bromide for chloride moves the absorption to 961 nm in **3a**. In the case of **2b** with the fluorinated (dpp-nacnac^{CF3})$^-$ ligand, the lowest energy transition shifts to 713 nm in **2b** and 738 nm in **3b**.

Electrochemical Studies of (dpp-nacnac^R)RhX$_2$(phdi). Electrochemical studies of **2** and **3** indicate facile two-electron reduction of the dihalide complexes to afford **1**. Figure 4 shows cyclic voltammetry data for complexes **1a**, **2a**, and **3a** in THF. As previously reported,[26] complex **1a** shows reversible one-electron reductive and oxidative processes at −2.03 V and +0.06 V vs $(Cp_2Fe)^{+/0}$ along with partially reversible reductive and oxidative features near the edges of the solvent window.

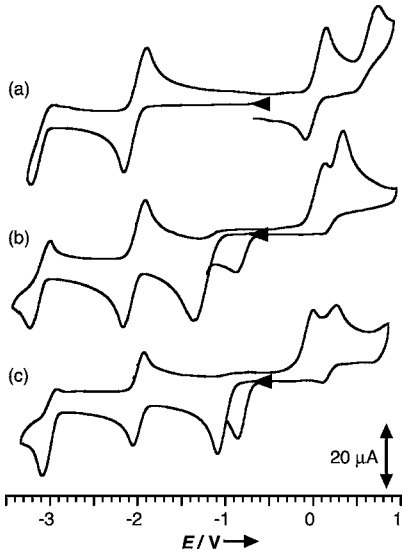

Figure 4. Cyclic voltammograms of (a) (dpp-nacnac^{CH3})Rh(phdi) (**1a**), (b) (dpp-nacnac^{CH3})RhCl$_2$(phdi) (**2a**), and (c) (dpp-nacnac^{CH3})RhBr$_2$(phdi) (**3a**) measured at 200 mV s^{-1}. All measurements made in THF with 1.0 mM analyte and 0.10 M (n-Bu_4N)PF_6 under N_2 or Ar. Potentials referenced to $(Cp_2Fe)^{+/0}$.

Scanning negatively, rhodium(III) dichloride, **2a**, shows a broad cathodic signal at −1.31 V vs $(Cp_2Fe)^{+/0}$, followed by reversible and partially reversible processes at −2.04 and −3.10 V, respectively. The anodic portion of the CV shows an irreversible peak at 0.24 V, which becomes slightly reversible at higher scan rates (>400 mV s^{-1}, i_{pc}/i_{pa} = 0.5 at 1600 mV s^{-1}) and gives rise to a daughter reduction at −0.88 V. An additional anodic process at 0.08 V is observed as a result of the irreversible reduction at −1.31 V. A 2:1 relative integration of the cathodic peak at −1.31 V to the cathodic portion of the process at −2.04 V as well as comparison to decamethylferrocene suggests that the signal at −1.31 V is a two-electron reduction of **2a**. Two-electron reduction, concomitant with halide dissociation, would convert **2a** to rhodium(I) complex **1a**, and this hypothesis is supported by the rest of the cyclic voltammogram for **2a**, which closely mirrors that of **1a**. Furthermore, the presence of 2 equiv of (n-Bu_4N)Cl in solution with **1a** caused changes in the anodic region to strongly resemble that of **2a** (see Supporting Information). Similarly, the CV of **3a** displays a two-electron cathodic peak at −1.19 V followed by the same one-electron reductive and oxidative processes observed for **1a**. Table 3 summarizes the electrochemical data for **1**, **2**, and **3**. The fluorinated complexes **2b** and **3b** exhibited similar behavior, and their cyclic voltammograms are included in the Supporting Information.

Table 3. Electrochemical Data for (dpp-nacnac^{CH3})Rh(phdi) (1a), (dpp-nacnac^{CF3})Rh(phdi) (1b), (dpp-nacnac^{CH3})RhCl$_2$(phdi) (2a), (dpp-nacnac^{CF3})RhCl$_2$(phdi) (2b), (dpp-nacnac^{CH3})RhBr$_2$(phdi) (3a), and (dpp-nacnac^{CF3})RhBr$_2$(phdi) (3b)

complex	$E_1°'$	$E_2°'$	E_3(pc)′	$E_4°'$	E_4(pa)′	E_5(pa)′
1a	−3.08	−2.03		0.06		0.79
1b	−2.69[a]	−1.79		0.37		0.75
2a	−3.10	−2.04	−1.31		0.24	
2b	−2.79[a]	−1.73	−1.11		1.12	
3a	−3.10	−2.04	−1.19		0.34	
3b	−2.74[a]	−1.72	−1.03		1.07	

[a]This reduction process had a significant enough return current to be measured as $E_{1/2}$ for compounds **1a**, **2a**, and **3a**, but is reported as E_{pc} for compounds **1b**, **2b**, and **3b**.

Reactions with I_2. Iodine adds to complex **1a**, without a formal oxidative addition to the metal center. Upon addition of I_2 to a solution of **1a**, a transition from blue to green-brown was accompanied with the appearance of a dark precipitate. The product of the reaction, (dpp-nacnac^{CH3})Rh(I_2)(phdi) (**4a**), was isolated as a brown solid and was recrystallized from a saturated CH_2Cl_2 solution. Figure 5 shows the molecular structure of **4a** as determined by single-crystal X-ray diffraction; Table 2 lists selected metrical parameters for the complex. The striking feature of the structure is an η^1-coordinated I_2 molecule at the apex of a square-pyramidal rhodium center. The I_2 molecule is coordinated in a linear fashion (Rh−I−I ~176°) with a long Rh−I distance of 2.67 Å and an I−I bond distance that is elongated significantly compared to free I_2 (3.01 Å in **4a** vs 2.72 Å for I_2 in the solid state).[38] There are no significant inter- or intramolecular interactions to the terminal iodine. The closest contact for the terminal iodine is to a hydrogen of a CH_2Cl_2 solvent at 3.24 Å; the nearest rhodium metal center is 7.51 Å away. The nitrogen donors of the (dpp-nacnac^{CH3})$^-$ and phdi ligands define the basal plane of the square pyramid; the

dx.doi.org/10.1021/ic300733j | Inorg. Chem. 2012, 51, 12122−12131

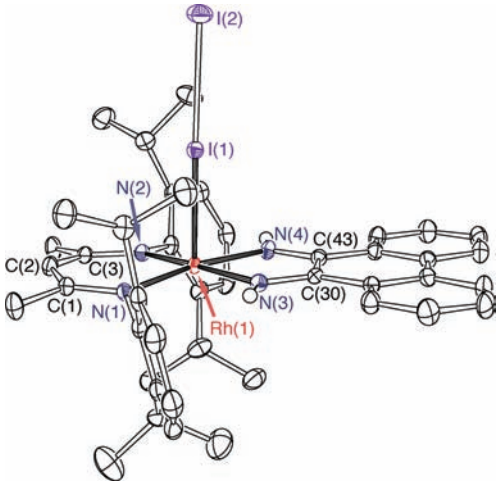

Figure 5. ORTEP diagram of (dpp-nacnac^{CH3})Rh(I_2)(phdi) (**4a**). Thermal ellipsoids are shown at 50% probability. Hydrogen atoms and solvent molecules are omitted for clarity.

Rh−N bond distances are longer than those of **1a**, but shorter than those observed for oxidized **2a**. Similarly, the C−N distances within the phdi ligand are intermediate between those in **1a** and **2a**. These two factors suggest that the rhodium center in **4a** is not fully oxidized to the formal rhodium(III) oxidation state but is less electron rich than in **1a**. The diisopropylphenyl substituents of the (dpp-nacnac^{CH3})$^-$ ligand are bent down and canted away from the coordinated I_2 molecule to partially block the distal side of the rhodium center.

Characterization of **4a** in solution by NMR spectroscopy revealed a dynamic coordination environment at room temperature, but when cooled to −50 °C, the spectrum is consistent with the solid-state structure. Notably, at low temperature there are two well-resolved methine resonances and four methyl resonances assignable to isopropyl groups above and below the basal plane of the square pyramid. Four aromatic proton resonances for the phdi ligand and one methyl resonance for the backbone of the (dpp-nacnac)$^-$ ligand are consistent with the approximate C_s symmetry of the square-pyramidal geometry observed in the solid state.

Iodine adduct **4a** could also be prepared by the reaction of dichloride **2a** with iodide salts. When **2a** was stirred with 10 equiv of LiI in CH_2Cl_2 for several days, complete conversion to **4a** was observed as shown in Scheme 3. Shorter reaction times or substoichiometric quantites of LiI resulted in partial conversion to **4a**. The ^{1}H NMR spectrum of these reaction mixtures revealed **4a** and a new unsymmetrical product proposed to be (dpp-nacnac^{CH3})RhICl(phdi) with trans halide ligands in a pseudo-octahedral geometry analogous to **2a**. This putative unsymmetrical species is not fluxional at room temperature, but shows two methine resonances for the isopropyl groups of the (dpp-nacnac^{CH3})$^-$ ligand, consistent with different halides above and below the equatorial plane. An equimolar mixture of **2a** and **4a** in CH_2Cl_2 at room temperature equilibrated to a mixture of all three species—**2a**, **4a** and putative (dpp-nacnac^{CH3})RhICl(phdi)—according to ^{1}H NMR spectroscopy.

Treatment of **1b** with 1 equiv of I_2 generated a mixture of a terminal rhodium-I_2 adduct and a rhodium(III) *trans*-diiodide complex, as shown in Scheme 3. A blue solution of **1b** underwent a similar color change to **1a** upon addition of I_2, changing from dark blue to dark green-brown, and the room

Scheme 3

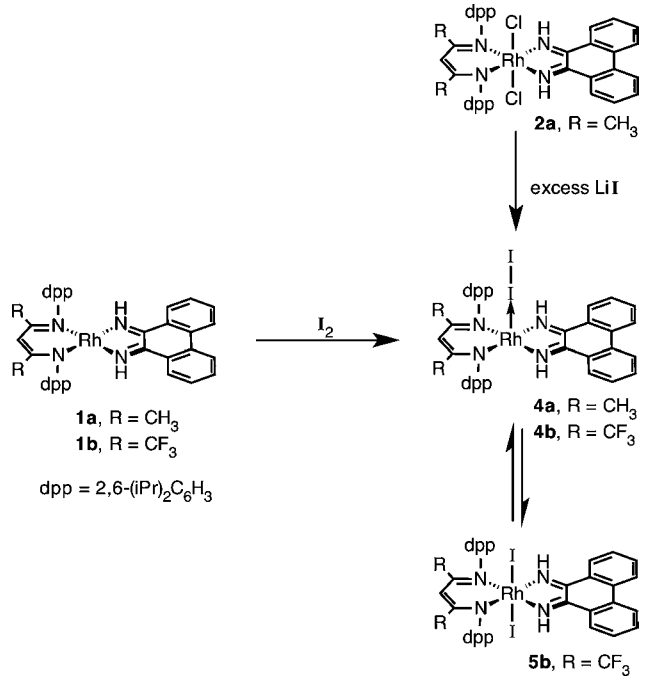

temperature ^{1}H NMR spectrum was broad. Upon cooling to −50 °C, two sets of peaks were revealed: one set similar to adduct **4a** and another set similar to oxidative addition products **2b** and **3b**. A singlet at 8.62 ppm and doublets at 8.10 and 6.90 ppm are characteristic of N−H and aromatic protons, respectively, of a phdi ligand in a complex similar to **4a**. Furthermore, peaks were observed corresponding to the isopropyl groups at similar shifts to **4a**. The largest deviation from **4a** in the proposed (dpp-nacnac^{CF3})Rh(I_2)(phdi) (**4b**) is in the methine proton on the (dpp-nacnac^{CF3})$^-$ backbone, whose resonance is shifted 0.52 ppm downfield, consistent with differences observed between fluorinated and nonfluorinated versions of **2** and **3**. The second set of resonances appear to correspond to a rhodium(III) complex resulting from oxidative addition of iodine, (dpp-nacnac^{CF3})RhI_2(phdi) (**5b**). A singlet at 9.95 ppm corresponding to the N−H of phdi is characteristic of a rhodium(III) complex. The other peaks associated with **5b** correspond closely to **3b**, including a singlet at 5.63 ppm corresponding to the (dpp-nacnac^{CF3})$^-$ methine proton. Upon warming, the resonances associated with **4b** and **5b** broaden and coalesce into a single set of broad resonances, consistent with exchange on the NMR time scale. The generally congested NMR spectrum and the effect of temperature on the equilibrium constant at temperatures below coalescence precluded determination of activation parameters by band shape analysis; however, the coalescence temperature for both the N−H and (dpp-nacnac^{CF3})$^-$ backbone C−H resonances was used to determine that $\Delta G^{\ddagger}$ for the oxidative addition reaction is approximately 12 kcal/mol at 0 °C.

Inducing Oxidative Addition of I_2. Hydrohalic acids react with **2**, **3**, and **4** to protonate the backbone of the (dpp-nacnac^{R})$^-$ ligand and afford cationic rhodium(III) dihalide complexes, as shown in Scheme 4. In the presence of excess HCl, the dark brown complex **2a** reacted with only 1 equiv, resulting in protonation of the (dpp-nacnac^{CH3})$^-$ backbone, without any change to the phdi ligand or to the metal center, affording the light orange product [(dpp-nacnacH^{CH3})-

dx.doi.org/10.1021/ic300733j | *Inorg. Chem.* 2012, 51, 12122−12131

Scheme 4

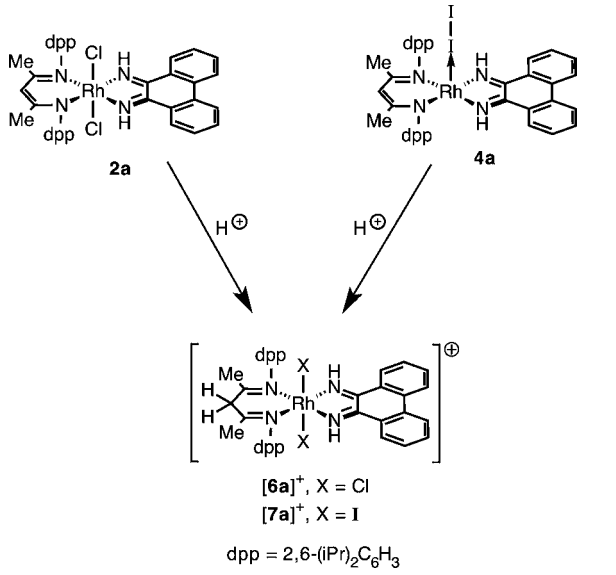

$RhCl_2(phdi)][Cl]$ ([**6a**][Cl]) in 87% yield. The ^1H NMR spectrum of the product revealed several diagnostic peaks. First, a singlet at 9.88 ppm and a doublet at 8.08 ppm are indicative of the phdi ligand on a rhodium(III) center and are shifted by less than 0.1 ppm from the corresponding peaks in **2a**. Second, the resonance corresponding to the proton in the (dpp-nacnac^{CH3})$^-$ backbone of **2a** was replaced with a singlet at 5.72 ppm that integrated to two protons, indicative of protonation to form the neutral (dpp-nacnacH^{CH3}) ligand. In the APCI mass spectrum of [**6a**]$^+$, peaks were observed for both [M]$^+$ at 797.1 amu and [M − H]$^+$ at 796.1 amu. Infrared spectroscopy showed a strong absorption at 1659 cm^{-1}, consistent with localized C═N double bonds that was not observed in **2a**. Finally, reaction of **2a** with acid to form [**6a**]$^+$ resulted in quenching of the low-energy CT band at 941 nm and the appearance of a peak at 470 nm (see Supporting Information). The compound [(dpp-nacnacH^{CH3})$RhCl_2$(phdi)][BF_4], [**6a**][BF_4] was synthesized similarly, using HBF_4·OEt_2 as the acid source. NMR, IR, and MS analysis confirmed congruence with the HCl product.

The addition of acid to solutions of I_2 adduct **4a** promoted cleavage of the I–I bond and oxidative addition of iodine to form the rhodium(III) cation, [(dpp-nacnacH^{CH3})-RhI_2(phdi)]$^+$, [**7a**]$^+$. Dark green **4a** reacted with a slight excess of HBF_4·OEt_2 to give a dark red-orange solution. The ^1H NMR spectrum of the crude reaction mixture indicated that the reaction produced a single major product, which was isolated as a red solid in 77% yield. The proton and carbon NMR spectra of the product were markedly similar to that of [**6a**]$^+$, implying that protonation of the (dpp-nacnac^{CH3})$^-$ ligand had induced oxidative addition of I_2 to form [(dpp-nacnacH^{CH3})-RhI_2(phdi)][BF_4] ([**7a**][BF_4]). Because of the proclivity of the iodine/iodide compounds to fragment upon ionization in the MS, the highest mass observable corresponded to the parent compound **1a**. However, NMR and IR spectra support the notion that [**7a**][BF_4] is analogous to [**6a**][BF_4]. Notably, the rhodium cation of [**7a**]$^+$ shows C_{2v} symmetry with four equivalent isopropyl groups on the (dpp-nacnacH^{CH3}) ligand in the room-temperature ^1H NMR spectrum. The protons of the (dpp-nacnacH^{CH3}) backbone resonated at 5.28 ppm and the NH protons of the phdi ligand were shifted to 10.16 ppm, consistent with a phdi ligand coordinated to rhodium(III).

DISCUSSION

Halogen Addition to (dpp-nacnac^R)Rh(phdi). The reaction of rhodium complexes **1a** and **1b** with chlorine (as $PhICl_2$) and bromine is a textbook oxidative addition reaction. The halogens add to square-planar **1a** or **1b** to afford octahedral rhodium(III) complexes **2a** or **2b** (X = Cl) and **3a** or **3b** (X = Br). The rhodium(III) oxidation state observed in the products is well-defined since the phdi ligand is present in the oxidized, quinone-like oxidation state. This clarity stands in contrast with rhodium complexes **1a** and **1b**, where a reduced rhodium(I) metal coordinated to a quinone-like phdi ligand leads to ambiguity in the experimental metal and ligand oxidation states.

Iodine addition to **1a** and **1b** provides further insight into more subtle electronic and steric factors governing the reactivity of these complexes. In the case of **1a**, (dpp-nacnac^{CH3})Rh(phdi), the addition of I_2 afforded the terminal Lewis acid–base adduct **4a**, (dpp-nacnac^{CH3})Rh(I_2)(phdi). The Rh–I_2 fragment is isoelectronic with the triiodide anion, I_3^-, with the (dpp-nacnac^{CH3})Rh(phdi) fragment serving as a Lewis base and the I_2 fragment as a Lewis acid. This adduct can also be viewed as a model for the first step in the oxidative addition of halogens to the rhodium(I) metal center; however, it is important to point out that **4a** is not a kinetic product since it may be prepared by a metathesis route from **2a** and lithium iodide. Whereas iodine addition to **1a** strongly favors adduct **4a**, the analogous reaction with **1b**, (dpp-nacnac^{CF3})Rh(phdi), results in an equilibrium mixture of the iodine adduct **4b**, (dpp-nacnac^{CF3})Rh(I_2)(phdi), and the iodine oxidative addition product **5b**, (dpp-nacnac^{CF3})RhI_2(phdi). NMR analysis of the product mixture from **1b** and I_2 shows dynamic behavior at room temperature that can be arrested upon cooling to −50 °C where both Lewis adduct **4b** and oxidative addition product **5b** can be observed in the low-temperature ^1H NMR spectrum. That the spectroscopic signatures for these isomers coalesce at warmer temperatures confirms that **4b** and **5b** are in equilibrium and that the I_2 adduct **4b** is not a kinetic product along the path to formation of **5b**.

An interesting feature of I_2 addition to **1a** and **1b** is the relative position of the equilibrium between iodine adduct formation and iodine oxidative addition for analogous complexes of the (dpp-nacnac^{CH3})$^-$ and (dpp-nacnac^{CF3})$^-$ ligands. It seems counterintuitive that iodine addition to **1a** strongly favors adduct **4a**, while the analogous reaction with **1b**, (dpp-nacnac^{CF3})Rh(phdi), results in an equilibrium mixture of the iodine adduct **4b**, (dpp-nacnac^{CF3})Rh(I_2)(phdi), and the iodine oxidative addition product **5b**, (dpp-nacnac^{CF3})-RhI_2(phdi). The more electron rich (dpp-nacnac^{CH3})$^-$ ligand would normally be expected to make the rhodium center more electron rich and thus promote oxidative addition, whereas the (dpp-nacnac^{CF3})$^-$ ligand should make the rhodium center more electron poor and thus disfavor oxidative addition. Such a model is supported by studies of I_2 addition to gold-phosphine complexes in which more electron-rich phosphines favored oxidative addition.[39] To understand the effect of (dpp-nacnac^R)$^-$ ligand on I_2 addition to **1a** and **1b**, the nature of the equilibrium between the I_2 adduct, (dpp-nacnac^R)Rh(I_2)-(phdi), and the oxidative addition product, (dpp-nacnac^R)-RhI_2(phdi) must be carefully examined. As shown in Scheme 5, formation of the Lewis acid–base adduct **4** requires the

dx.doi.org/10.1021/ic300733j | Inorg. Chem. 2012, 51, 12122–12131

Scheme 5

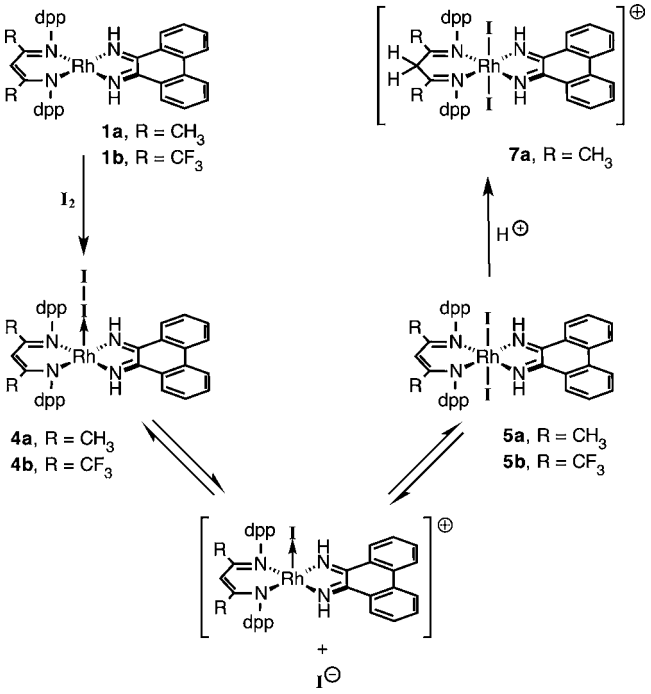

donation of two electrons from the rhodium(I) center to the σ^* orbital of I_2; thus, in **4** the rhodium center is partially oxidized relative to the rhodium center in **1**, a proposal that is supported by the structural features of **4a**. Conversion of **4** into putative (dpp-nacnac^R)RhI$_2$(phdi) (**5**) can then proceed via heterolytic cleavage of the I–I bond followed by iodide coordination to the trans site of the rhodium center. If these processes are reversible, then the position of the equilibrium between **4** and **5** is determined by the relative electrophilicity of the rhodium and iodine centers in the putative cation (dpp-nacnac^R)RhI(phdi)$^+$, generated upon dissociation of I^-. In the complex with the (dpp-nacnac^{CH3})$^-$ ligand, the rhodium center of [(dpp-nacnac^{CH3})RhI(phdi)]$^+$ (shown in Scheme 5) is less Lewis acidic than the iodide ligand so the free iodide coordinates to reform the I–I bond and thus favors **4a**. In the complex with the less electron donating (dpp-nacnac^{CF3})$^-$ ligand, the rhodium of [(dpp-nacnac^{CF3})RhI(phdi)]$^+$ center is more Lewis acidic, so coordination of the free iodide to the iodide ligand and rhodium center is isoenergetic and an equilibrium is established between **4b** and **5b**. The effect of acid on the I_2 addition to **1** supports the contention that rhodium electrophilicity controls the equilibrium between **4** and **5** since the addition of HBF_4 to iodine adduct **4a** resulted in the cleavage of the I–I bond and the formation of the diiodide cation [(dpp-nacnacH^{CH3})RhI$_2$(phdi)]$^+$, [**7a**]$^+$. Protonation of the (dpp-nacnac^{CH3})$^-$ ligand forms the neutral (dpp-nacnacH^{CH3}) diimine ligand, which is less electron-rich than the (dpp-nacnac^{CH3})$^-$ anion. As a result, the rhodium center becomes more Lewis acidic and favors complete oxidative addition of iodine to the rhodium center.

Charge Transfer in (dpp-nacnac^R)Rh(phdi) and (dpp-nacnac^R)RhX$_2$(phdi). The electronic absorption spectra of reduced rhodium complexes **1** and oxidized complexes **2** and **3** show strong charge-transfer transitions in the visible portion of the electromagnetic spectrum. As previously reported, the UV–vis spectra of **1a** and **1b** are dominated by intense optical transitions at 593 and 587 nm, respectively. The intensity of these absorptions (ε > 21,000 M^{-1} cm^{-1}) clearly identify them as charge transfer bands while the negligible dependence of the band energy on the (dpp-nacnac^R)$^-$ ligand (ΔE_{nacnac} = 173 cm^{-1}) suggests that it is likely a metal-to-ligand charge-transfer (MLCT) transition involving the rhodium center as the electron donor and the phdi ligand as the electron acceptor. In contrast, the low-energy absorptions in the UV–vis spectra of **2** and **3** are characterized by a weaker intensity ($\varepsilon \cong$ 2300 M^{-1} cm^{-1}), but they show a profound dependence on the (dpp-nacnac^R)$^-$ ligand ($\Delta E_{nacnac} \cong$ 3000 cm^{-1}) and a relatively small dependence on the halogen (ΔE_{X2} < 500 cm^{-1}). These absorption bands appear at lower energy in complexes **2a** and **3a** containing the (dpp-nacnac^{CH3})$^-$ ligand than in complexes **2b** and **3b** containing the (dpp-nacnac^{CF3})$^-$ ligand. Together these data suggest that the low-energy absorption band in **2** and **3** is a ligand-to-ligand charge-transfer (LL′CT) transition involving the transfer of an electron from the (dpp-nacnac^R)$^-$ donor ligand to the phdi acceptor ligand. This is further supported by disappearance of this low-energy absorption in [**6a**]$^+$ where the (dpp-nacnac^R)$^-$ backbone has been protonated.

CONCLUSIONS

The oxidative addition reactivity of **1a** and **1b** with halogen reagents highlight that these complexes react as "normal" square-planar rhodium(I) complexes despite the electronic ambiguity arising from the juxtaposition of an electron-rich rhodium center and an electron-poor phdi ligand. The surprising reactivity of I_2 with **1a** and **1b** and the isolation of the I_2 adduct **4a** also highlight the subtle effects that auxiliary ligand electronics can have on the position of oxidative addition equilibria. The incomplete oxidative addition of I_2 to **1a** and **1b** is not necessarily determined by an inability of I_2 to oxidize the rhodium center, but rather it can be strongly influenced by the preference for the iodide Lewis base to bind at the iodide ligand (reforming the I–I bond) rather than at the rhodium center (to complete the oxidative addition reaction).

The oxidative addition of halogens to **1a** and **1b** extensively affects the electronic absorption properties of the rhodium products. Whereas the electronic spectra of **1a** and **1b** are dominated by MLCT transitions at relatively high energy involving the rhodium center and the phdi ligand, oxidation to **2** and **3** turns on a low-energy LL′CT transition in which the (dpp-nacnac^R)$^-$ ligand serves as the electron donor and the phdi ligand serves as the electron acceptor. Such charge-transfer transitions suggest intriguing possibilities for photochemical applications especially given the apparent wide tunability in the wavelength of light absorption.

ASSOCIATED CONTENT

Supporting Information

Cyclic voltammograms of **1** in the presence of [*n*-Bu$_4$N][Cl], **2b**, and **3b**. Electronic absorption spectrum of [**6a**][BF$_4$]. NMR spectra for **4a**, **4b**, [**6a**][BF$_4$], [**7a**][BF$_4$]. This material is available free of charge via the Internet at http://pubs.acs.org.

AUTHOR INFORMATION

Corresponding Author

*E-mail: aheyduk@uci.edu.

Notes

The authors declare no competing financial interest.

■ ACKNOWLEDGMENTS

This work was supported by the UCI School of Physical Sciences Center for Solar Energy. A.F.H. is a Camille Dreyfus Teacher-Scholar. Rhodium starting material was donated by Heraeus.

■ REFERENCES

(1) Crabtree, R. H. *The Organometallic Chemistry of the Transition Metals*; Wiley: Hoboken, NJ, 2009.
(2) Miessler, G. L.; Tarr, D. A. *Inorganic Chemistry*; Pearson Prentice Hall: Upper Saddle River, NJ, 2011.
(3) Rendina, L. M.; Puddephatt, R. J. *Chem. Rev.* **1997**, *97*, 1735−1754.
(4) Winterton, N. *Annu. Rep. Prog. Chem., Sect. A: Inorg. Chem.* **2000**, *96*, 557−623.
(5) Cotton, F. A.; Wilkinson, G.; Murillo, C. A.; Bochmann, M. *Advanced Inorganic Chemistry*, 6th ed.; Wiley: New York, 1999.
(6) Skinner, C. E.; Jones, M. M. *J. Am. Chem. Soc.* **1969**, *91*, 4405−4408.
(7) Morgan, K. A.; Jones, M. M. *J. Inorg. Nucl. Chem.* **1972**, *34*, 275−296.
(8) Jones, M. M.; Morgan, K. A. *J. Inorg. Nucl. Chem.* **1972**, *34*, 259−274.
(9) Van Zyl, G. J.; Lamprecht, G. J.; Leipoldt, J. G. *Inorg. Chim. Acta* **1987**, *129*, 35−37.
(10) Bickelhaupt, F. M.; Baerends, E. J.; Ravenek, W. *Inorg. Chem.* **1990**, *29*, 350−354.
(11) Chrzanowski, L. S. V.; Lutz, M.; Spek, A. L.; Suijkerbuijk, B. M. J. M.; Klein Gebbink, R. J. M. *Acta Crystallogr.* **2007**, *E63*, m1223−m1225.
(12) van Koten, G.; van Beek, J. A. M.; Dekker, G. P. C. M.; Wissing, E.; Zoutberg, M. C.; Stam, C. H. *J. Organomet. Chem.* **1990**, *394*, 659−678.
(13) van Beek, J. A. M.; van Koten, G.; Smeets, W. J. J.; Spek, A. L. *J. Am. Chem. Soc.* **1986**, *108*, 5010−5011.
(14) Gossage, R. A.; Ryabov, A. D.; Spek, A. L.; Stufkens, D. J.; van Beek, J. A. M.; van Eldik, R.; van Koten, G. *J. Am. Chem. Soc.* **1999**, *121*, 2488−2497.
(15) van Koten, G. *Pure Appl. Chem.* **1990**, *62*, 1155−1159.
(16) Makiura, R.; Nagasawa, I.; Kimura, N.; Ishimaru, S.; Kitagawa, H.; Ikeda, R. *Chem. Commun.* **2001**, 1642−1643.
(17) Imhoff, P.; Gülpen, J. H.; Vrieze, K.; Smeets, W. J. J.; Spek, A. L.; Elsevier, C. J. *Inorg. Chim. Acta* **1995**, *235*, 77−88.
(18) Braunstein, P.; Chauvin, Y.; Fischer, J.; Olivier, H.; Strohmann, C.; Toronto, D. V. *New J. Chem.* **2000**, *24*, 437−445.
(19) Cuervo, D.; Díez, J.; Gamasa, M. P.; Gimeno, J.; Paredes, P. *Eur. J. Inorg. Chem.* **2006**, 599−608.
(20) Haines, L. M. *Inorg. Chem.* **1971**, *10*, 1693−1699.
(21) Hahn, C.; Spiegler, M.; Herdtweck, E.; Taube, R. *Eur. J. Inorg. Chem.* **1999**, 435−440.
(22) Das, P.; Sharma, M.; Kumari, N.; Konwar, D.; Dutta, D. K. *Appl. Organomet. Chem.* **2002**, *16*, 302−306.
(23) Yahav, A.; Goldberg, I.; Vigalok, A. *Organometallics* **2005**, *24*, 5654−5659.
(24) Cotton, F. A.; Dikarev, E. V.; Petrukhina, M. A. *Angew. Chem., Int. Ed.* **2000**, *39*, 2362−2364.
(25) Fukuzumi, S.; Nishizawa, N.; Tanaka, T. *Bull. Chem. Soc. Jpn.* **1982**, *55*, 2886−2891.
(26) Shaffer, D. W.; Ryken, S. A.; Zarkesh, R. A.; Heyduk, A. F. *Inorg. Chem.* **2011**, *50*, 13−21.
(27) Lucas, H. J.; Kennedy, E. R. *Org. Synth.* **1942**, *22*, 69.
(28) Connelly, N. G.; Geiger, W. E. *Chem. Rev.* **1996**, *96*, 877−910.
(29) Farrugia, L. J. *J. Appl. Crystallogr.* **1997**, *30*, 565−565.
(30) Masuda, J. D.; Stephan, D. W. *Can. J. Chem.* **2005**, *83*, 324−327.
(31) Budzelaar, P. H. M.; de Gelder, R.; Gal, A. W. *Organometallics* **1998**, *17*, 4121−4123.
(32) Blacker, A. J.; Clot, E.; Duckett, S. B.; Eisenstein, O.; Grace, J.; Nova, A.; Perutz, R. N.; Taylor, D. J.; Whitwood, A. C. *Chem. Commun.* **2009**, 6801−6803.
(33) Broring, M.; Consul Tejero, E.; Pfister, A.; Brandt, C. D.; Perez Torrente, J. J. *Chem. Commun.* **2002**, 3058−3059.
(34) Efe, G. E.; Schlemper, E. O. *Polyhedron* **1992**, *11*, 2447−2458.
(35) Ganguly, S.; Manivannan, V.; Chakravorty, A. *Dalton Trans.* **1998**, 461−466.
(36) Konrad, F.; Lloret Fillol, J.; Wadepohl, H.; Gade, L. H. *Inorg. Chem.* **2009**, *48*, 8523−8535.
(37) Hoogervorst, W. J.; Goubitz, K.; Fraanje, J.; Lutz, M.; Spek, A. L.; Ernsting, J. M.; Cornelis, J. *Organometallics* **2004**, *23*, 4550−4563.
(38) Greenwood, N. N.; Earnshaw, A. *Chemistry of the Elements*, 2nd ed.; Butterworth-Heinemann: Oxford, U.K., 1997.
(39) Schneider, D.; Schier, A.; Schmidbaur, H. *Dalton Trans.* **2004**, 1995−2005.